Biodistribution, Tumor Detection, and Radiation Dosimetry of ^{18}F-5-Fluoro-2′-Deoxycytidine with Tetrahydrouridine in Solid Tumors

Colin R. Young[1], Stephen Adler[2], Janet F. Eary[3], M. Liza Lindenberg[4], Paula M. Jacobs[3], Jerry Collins[5], Shivaani Kummar[6], Karen A. Kurdziel[4], Peter L. Choyke[4], and Esther Mena[4]

[1]Department of Radiology, Walter Reed National Military Medical Center, Bethesda, Maryland; [2]Clinical Research Directorate/ Clinical Monitoring Research Program, Leidos Biomedical Research, Inc., National Cancer Institute, Frederick, Maryland; [3]Cancer Imaging Program, National Cancer Institute, National Institutes of Health, Bethesda, Maryland; [4]Molecular Imaging Program, National Cancer Institute, National Institutes of Health, Bethesda, Maryland; [5]Developmental Therapeutics Program, National Cancer Institute, National Institutes of Health, Bethesda, Maryland; and [6]Stanford University School of Medicine, Palo Alto, California

In preclinical studies, 5-fluoro-2′-deoxycytidine (FdCyd), an inhibitor of DNA methyltransferase and DNA hypermethylation, has shown treatment efficacy against multiple malignancies by suppressing epigenetic hypermethylation in tumor cells. Several ongoing clinical trials are using FdCyd, and although some patients may respond to this drug, in most patients it is ineffective. Thus, establishing a noninvasive imaging modality to evaluate the distribution of the drug may provide insight into the variable responses. A novel experimental radiopharmaceutical, ^{18}F-labeled FdCyd, was developed as a companion imaging agent to the nonradioactive form of the drug, FdCyd. We present the first-in-humans radiation dosimetry results and biodistribution of ^{18}F-FdCyd, administered along with tetrahydrouridine, an inhibitor of cytidine/deoxycytidine deaminase, in patients with a variety of solid tumors undergoing FdCyd therapy. **Methods:** This phase 0 imaging trial examined the ^{18}F-FdCyd biodistribution and radiation dosimetry in 5 human subjects enrolled in companion therapy trials. In each subject, 4 sequential PET scans were acquired to estimate whole-body and individual organ effective dose, using OLINDA/EXM, version 1.0. Tumor-to-background ratios were also calculated for the tumor sites visualized on PET/CT imaging. **Results:** The average whole-body effective dose for the experimental radiopharmaceutical ^{18}F-FdCyd administered in conjunction with tetrahydrouridine was 2.12E−02 ± 4.15E−03 mSv/ MBq. This is similar to the radiation dose estimates for ^{18}F-FDG PET. The critical organ, with the highest absorbed radiation dose, was the urinary bladder wall at 7.96E−02 mSv/MBq. Other organ doses of note were the liver (6.02E−02mSv/MBq), kidneys (5.26E −02 mSv/MBq), and gallbladder (4.05E−02 mSv/MBq). Tumor target-to-background ratios ranged from 2.4 to 1.4, which potentially enable tumor visualization in static PET images. **Conclusion:** This phase 0 imaging clinical trial provides evidence that ^{18}F-FdCyd administered in conjunction with tetrahydrouridine yields acceptable individual organ and whole-body effective doses, as well as modest tumor-to-background ratios that potentially enable tumor visualization. Dose estimates for ^{18}F-FdCyd are comparable to those for other PET radiopharmaceuticals, such as ^{18}F-FDG. Further studies with larger study populations are warranted to assess ^{18}F-FdCyd imaging as a predictor of FdCyd treatment effectiveness.

Key Words: ^{18}F-FdCyd; tetrahydrouridine; PET imaging; cancer; molecular imaging

A relation between malignancy and DNA methylation was recognized a few decades ago (*1*). DNA methyltransferase expression is elevated in most cancers, resulting in epigenetic alterations in the cancer cell genome (*2*). One form of epigenetic modification observed in cancer cells is alterations in DNA methylation that alter regulation of gene transcription (*2*). Cancer cells often demonstrate global DNA hypomethylation leading to genomic instability, as well as foci of hypermethylation, particularly within CpG islands associated with tumor suppressor genes, resulting in tumor suppressor gene silencing and thus promoting tumor growth (*3*).

FdCyd, 5-fluoro-2′-deoxycytidine, is an antineoplastic agent that inhibits DNA methyltransferase and DNA methylation by forming a covalent bond with the enzyme after incorporation into DNA (*4*), resulting in reexpression of genes silenced by DNA hypermethylation. FdCyd can be phosphorylated to 5-fluoro-2′-deoxycytidylate (FdCMP) by deoxycytidine kinase and the nucleotide deaminated to 5-fluoro-2′-deoxyuridine 5′-monophosphate by deoxycytidylate (dCMP) deaminase (*5*). The activity of dCMP deaminase is reported to be higher in human malignancies than in normal tissues, which may result in selective cytotoxicity (*6,7*).

The efficacy of this developmental antineoplastic therapeutic agent, particularly in oral form, has been limited by its rapid degradation by cytidine deaminase (*8*). However, unlike prior versions of the drug such as 5-azacytidine and 5-aza-2′-deoxycytidine, the breakdown of FdCyd by cytidine deaminase can be largely suppressed by coadministration of 3,4,5,6-tetrahydrouridine, an inhibitor of cytidine/deoxycytidine deaminase (*9,10*), thus reducing enzymatic deamination, which has shown antitumor activity superior to other antimetabolites, such as 5-fluorouracil in preclinical models (*11,12*) and in early-phase clinical trials (*13*).

FdCyd and tetrahydrouridine have shown preliminary evidence of activity against solid tumors in early-phase trials, although not all patients showed clinical response (13). The establishment of a radiolabeled form to image the biodistribution in vivo during therapy may provide insight into the distribution of the therapeutic drug (3,14). Thus, to optimize the likelihood of FdCyd's clinical success against heterogeneous solid tumors, a companion diagnostic imaging agent, chemically identical to FdCyd and labeled with a PET tracer, could be useful in identifying tumors in which the drug is likely to accumulate and, therefore, where it could potentially be clinically more effective (15). Similar to other radiolabeled pyrimidine molecules, the limiting factor for imaging is the high background activity resulting from byproducts of pyrimidine catabolism, which in the case of radiolabeled FdCyd can be minimized with simultaneous administration of tetrahydrouridine (16). Thus, the present study was undertaken to better understand the biodistribution and radiation dosimetry of ^{18}F-labeled FdCyd with coadministration of tetrahydrouridine and to describe tumor uptake in a small cohort of patients with solid tumors who were concurrently participating in either a phase I or a phase II clinical trial of FdCyd and tetrahydrouridine

MATERIALS AND METHODS

Patients and Study Design

This study was approved by the local Institutional Review Board (Cancer Therapy Evaluation Program [CTEP] 8865; National Cancer Institute [NCI] protocol 12-C-0014) in compliance with all applicable Federal regulations governing the protection of human subjects, and informed consent was obtained from all patients before imaging. Biodistribution data from 5 subjects (3 men and 2 women; age range, 30–65 y old) who underwent ^{18}F-FdCyd PET were used for dosimetry estimates. The patients who were recruited were simultaneously participating in 1 of the 2 ongoing clinical therapeutic trials investigating FdCyd: a phase I trial (NCI protocol 12-C-0066; CTEP 9127; advanced solid tumors) and a phase II trial (NCI protocol 09-C-0214; CTEP 8351; head/neck, lung, breast, and urinary bladder neoplasms).

Radiopharmaceutical Production

Radioactive labeling of FdCyd with ^{18}F was performed at the University of Pennsylvania, in Philadelphia. The FdCyd was produced using 25 ± 3 mg of precursor, 2′-deoxycytidine, which was dissolved

in 8 mL of acetic acid, and 25 μL of the boron trifluoride acetic acid solution were added to the solution. Then, ^{18}F$_2$ was bubbled through it, with unreacted ^{18}F being captured by the KI solution. The activity was transferred to the evaporation vessel. The acetic acid was evaporated, and a second aliquot, 2 mL, of acetic acid was added and evaporated. The reaction product was transferred from the evaporation vial to the integrated high-pressure liquid chromatography injector port by the addition of 2 mL of the mobile-phase buffer (92:8 acetonitrile:deionized water). The high-pressure liquid chromatography was started, and the 5-formyl-2′-deoxycytidine was collected after approximately 45 min. After collection, the high-pressure liquid chromatography solvent was evaporated, and the final product was rinsed off the walls of the evaporation vessel using isotonic saline and transferred into a laminar flow or biosafety cabinet for final compounding. The drug substance was collected directly through a 0.2-μm sterilizing filter into a vented sterile vial. Samples were aseptically removed for analysis of product quality. The amount of injected drug was no more than 30 mg of 5-formyl-2′-deoxycytidine, providing a minimum specific activity of 80 mCi/mmol. A semiautomated synthesis unit was used so that each step in the procedure could be performed under computer control, minimizing the variance in the chemical reaction.

^{18}F-FdCyd PET Imaging

FdCyd and tetrahydrouridine were administered according to the specifications of the parent protocol, NCI clinical protocol 09-C-0214 (CTEP 8351) or NCI protocol 12-C-0066 (CTEP 9127). Briefly, an intravenous bolus of 20% of the total dose of tetrahydrouridine (total dose of tetrahydrouridine, 350 mg/m^2) was administered, followed by the remaining 80% of the dose, diluted in 250 mL of D5W, infused for 3 h or until the end of imaging. Twenty minutes after the start of intravenous tetrahydrouridine, and concurrent with or within 1 h after the start of the nonradioactive FdCyd therapeutic dose, the experimental PET radiopharmaceutical, ^{18}F-FdCyd (average dose, 140.6 ± 36.8 MBq), was administered intravenously over approximately 1 min. Three sequential static whole-body PET emission scans were performed from the top of the head to the upper thigh for up to 1 h. A fourth additional PET emission scan was acquired at about 2 h after injection. Low-dose CT scans (120 keV, 60 mAs) were acquired for attenuation correction and anatomic correlation.

Image Analysis

For each PET/CT examination, volumes of interest were manually drawn over all organs using MIM version 5.6.7 (MIM Software). When the entire organ volume could not be separated from the adjacent structures or the whole organ volume could not be delineated (e.g., heart wall, bone marrow, and muscle), a smaller volume of interest was drawn to estimate the organ activity concentration. For each PET examination, the activity concentration extracted from the volumes of interest was decay-corrected and normalized to the time of the initial dose injection. Tumor volumes of interest were manually drawn, as identified from prior diagnostic anatomic imaging studies and review of patient electronic medical records. Tumor SUV$_{max}$ was measured at 4 time points to assess biodistribution. Tumor-to-background ratios (TBRs) were also calculated.

Radiation Dosimetry

Time–activity curves for each organ region of interest were generated using Excel (Microsoft). An exponential decay function based on the half-life of ^{18}F was used to estimate the remainder of the time–activity curve after the
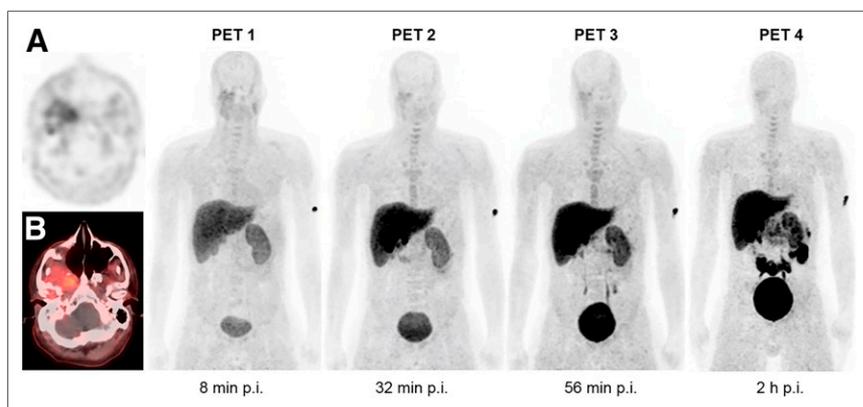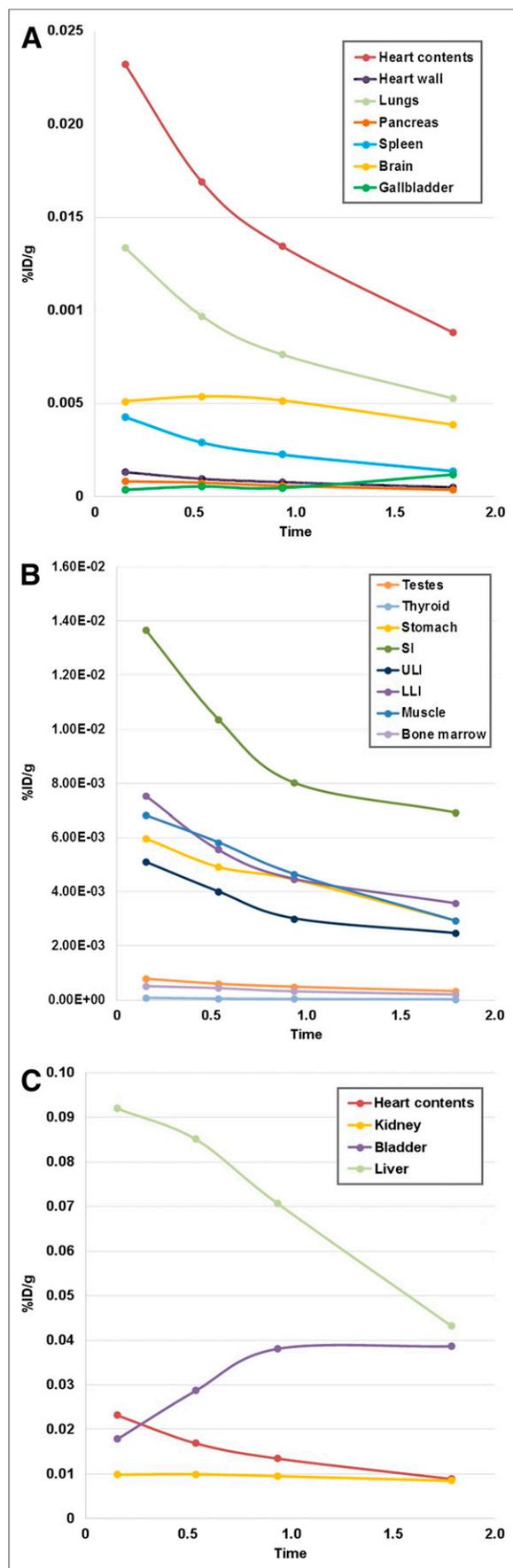

FIGURE 1. Maximum-intensity-projection PET imaging sequence after ^{18}F-FdCyd injection in patient 2. Images demonstrate physiologic uptake in liver, gallbladder, kidneys, urinary bladder, small intestine, and mildly in bone marrow. There is modest tumor uptake in histologically confirmed spindle cell carcinoma at right parapharyngeal and masticator spaces, best seen on axial PET (A) and PET/CT (B). p.i. = after injection.

FIGURE 2. Mean biodistribution curves plotted for percentage injected dose per gram of organ mass vs. time. (A) Organs with higher uptake. (B) Organs with lower uptake. (C) Increasing urinary bladder activity. LLI = lower large intestine; SI = small intestine; ULI = upper large intestine; %ID/g = percentage injected dose per gram of organ mass.

final time point. Normal organ radioactivity residence times were obtained by integrating the area under each time–activity curve. The residence times were entered into the kinetic input field in OLINDA/EXM version 1.0 (Vanderbilt University), which enabled calculation of individual-organ and whole-body effective doses. In the OLINDA model input form, the appropriate sex model was selected for each patient. No bladder-voiding or gastrointestinal models were used because of the short half-life of ^{18}F.

RESULTS

Tumor types represented in this study included head and neck cancer ($n = 2$), non–small cell lung cancer ($n = 2$), and hepatocellular carcinoma ($n = 1$). Patients had at least 1 target lesion measuring 1 cm or larger. Approximately 140.6 ± 36.8 MBq (~3.8 ± 0.9 mCi; range, 2.1–5 mCi) of ^{18}F-FdCyd was infused intravenously. Figure 1 shows maximum-intensity-projection ^{18}F-FDCyd PET images over time in a representative patient. The activity from the blood pool cleared rapidly, with evidence of hepatic and renal routes of excretion and radiotracer accumulation within the bladder. Physiologic radiotracer uptake was seen in the liver and small intestine. Time–activity curves for individual normal organs are shown in Figure 2.

Estimates of whole-body effective dose ranged from 1.86E−02 to 2.80E−02 mSv/MBq, with an average of 2.12E−02 ± 4.15E−03. The urinary bladder wall received the highest individual-organ dose, at 7.96E−02 mSv/MBq. Other organ doses of note were the liver (6.02E−02 mSv/MBq), kidneys (5.26E−02 mSv/MBq), and gallbladder (4.05E−02 mSv/MBq). Individual-organ and whole-body effective doses are shown in Table 1.

Four of the 5 patients showed visual tumor uptake, except for patient 5, whose target tumor was within the liver and obscured by the high background uptake of the liver. The average tumor SUV$_{max}$ was 3.3 (range, 2.6–3.9) for the first scan (average time, 9 min; range, 6–15 min), 2.4 (range, 2.0–3.1) for the second scan (average time, 32 min; range, 29–37 min), 2.1 (range, 1.9–2.1) for the third scan (average time, 56 min; range, 52–64 min), and 1.8 (range, 1.7–1.8) for the delayed scan at about 2 h after injection (average, 107 min; range, 86 min to 2 h), with calculated TBRs of 1.8, 1.7, 1.5, and 1.7, respectively. The patient-specific clinical information and tumor TBRs are detailed in Table 2.

DISCUSSION

The cytidine analog FdCyd has shown treatment efficacy in preclinical studies of solid and hematologic tumors (11). In the clinical setting, FdCyd was studied in combination with a fixed dose of tetrahydrouridine in a multicenter phase I study including 58 patients with advanced solid tumors (13); response data from 40 of those patients showed partial response for about 15 mo in 1 of the patients, and stable disease in 20 patients (13). Multiple factors have hampered the clinical effectiveness of FdCyd. The principal limiting factor in FdCyd activity is its rapid degradation by cytidine deaminase (8), leading to a very short half-life in circulation; however, this enzyme can be largely suppressed by

TABLE 1
Dosimetry Estimates in mSv/MBq

Site	Average	SD
Adrenals	1.83E−02	9.30E−03
Brain	8.17E−03	2.04E−03
Breasts	1.03E−02	1.01E−02
Gallbladder wall	4.05E−02	7.55E−03
Lower large intestine wall	2.52E−02	7.82E−03
Small intestine	2.13E−02	4.57E−03
Stomach wall	1.90E−02	3.27E−03
Upper large intestine wall	2.04E−02	6.43E−03
Heart wall	1.10E−02	1.82E−03
Kidneys	5.26E−02	2.23E−02
Liver	6.02E−02	2.74E−02
Lungs	1.82E−02	7.10E−03
Muscle	1.16E−02	1.35E−03
Ovaries	1.57E−02	2.22E−03
Pancreas	1.63E−02	4.27E−03
Red marrow	1.14E−02	2.19E−03
Osteogenic cells	1.71E−02	6.41E−03
Skin	8.65E−03	1.19E−03
Spleen	1.69E−02	5.55E−03
Testes	1.03E−02	2.38E−03
Thymus	1.12E−02	3.01E−03
Thyroid	8.23E−03	4.39E−03
Urinary bladder wall	7.96E−02	5.24E−02
Uterus	1.63E−02	4.99E−03
Effective dose	2.12E−02	4.15E−03

coadministration of 3,4,5,6-tetrahydrouridine, which greatly prolongs the clearance of the FdCyd (16). This is the first-in-humans study using ^{18}F-FdCyd and tetrahydrouridine PET/CT imaging presenting biodistribution and dosimetry data from 5 patients with solid tumors undergoing therapeutic trials with FdCyd. The intent of imaging ^{18}F-FdCyd in combination with tetrahydrouridine was to determine whether it would result in decreased background activity, and thus achieve acceptable TBRs, sufficient for tumor imaging. Similarly, other groups have used enzymatic inhibitor coadministration with developmental imaging agents as a rational approach to minimize undesirable background activity from radiopharmaceutical catabolism to improve TBR, that is, disulfiram mitigating defluorination in ^{18}F-FCWAY PET imaging (17). Other potential factors limiting drug effectiveness include heterogeneity of methylation patterns and limitations in the ability to deliver the drug in sufficient concentrations. ^{18}F-FdCyd was developed as a companion imaging agent to therapeutic FdCyd to provide a method for better patient selection. The aim of the study was to obtain preliminary safety data, human dosimetry, and biodistribution before deploying the agent on a wider basis.

The estimated whole-body effective dose for ^{18}F-FdCyd was acceptable, with a mean of 2.1E−02 mSv/MBq, similar to ^{18}F-FDG (18), which has an estimated whole-body effective dose of 1.9E−02 mSv/MBq (19). The effective dose was also similar to another ^{18}F-labeled developmental radiopharmaceutical, ^{18}F-fluoro-dihydrotestosterone, with an estimated whole-body effective dose of 1.8E−02 mSv/MBq (20). The largest estimated target organ dose for ^{18}F-FdCyd and tetrahydrouridine was the urinary bladder wall (7.96E−02 mSv/MBq), which was slightly less than the estimated dose to the urinary bladder wall in ^{18}F-FDG (8.65E−02 mSv/MBq) (21). With ^{18}F-FdCyd plus tetrahydrouridine, other high absorbed doses were found in the liver (6.02E−02mSv/MBq), the kidneys (5.26E−02 mSv/MBq), and the gallbladder (4.05E−02 mSv/MBq). These values modestly exceed those observed for corresponding organs with ^{18}F-FDG: 1.57E−02, 2.00E−02, and 1.32E−02 mSv/MBq, respectively (21). Although slightly higher, these doses do not approach regulatory limits.

The ^{18}F-FdCyd TBRs ranged from 2.4 to 1.4 (in $n = 4$), depending of type of tumor and scan time (Table 2). In 1 subject with a hepatocellular carcinoma, the tumor was not visualized because of intense liver background activity; thus, the TBR was not calculated. The minimal PET TBR necessary for detection depends on many factors such as imaging system and scan time; however, prior studies have demonstrated that a TBR of 3.0 can potentially detect a lesion as small as 0.4 mL and that a TBR of 1.85 can potentially detect a lesion as small as 0.5 mL (21,22). Our preliminary data show that ^{18}F-FdCyd PET imaging with tetrahydrouridine provides sufficient TBRs for detection of multiple types and sizes of tumors.

TABLE 2
Patient Demographics and TBR of Target Lesions on PET at 4 Time Points After Injection

Age (y)	Sex	Diagnosis	TBR			
			~9 min	~32 min	~56 min	~2 h
67	M	Left parotid adenosquamous cell carcinoma	1.4	1.5	1.5	1.6
30	M	Right parapharyngeal spindle cell carcinoma	1.9	1.7	1.7	1.6
65	F	Non–small cell lung cancer	1.4	1.4	1.5	1.7
51	F	Non–small cell lung cancer	2.4	2.1	1.6	2.0
63	M	Hepatocellular carcinoma	NA	NA	NA	NA

NA = not applicable: patient 5's tumor was within liver, and activity within tumor was not clearly discernable from remainder of liver parenchyma. Therefore, TBRs were not included for this subject because of concern about reporting misleading values in setting of high background/surrounding liver uptake.

The biodistribution and dosimetry estimates of ^{18}F-FdCyd revealed that the mechanism of radiopharmaceutical excretion is both renal and hepatic, thus limiting use for tumor detection in these 2 organs.

CONCLUSION

This phase 0, first-in-humans, clinical study provides evidence that PET imaging with ^{18}F-FdCyd and tetrahydrouridine is feasible and safe, with acceptable target organ and whole-body effective radiation doses, and produces modest TBRs sufficient for tumor localization. This study also provides dose estimates for ^{18}F-FdCyd that are comparable to those of other PET radiopharmaceuticals, such as ^{18}F-FDG. Further studies using ^{18}F-FdCyd in larger trials may be helpful to investigate its ability to enable selection of suitable candidates for FdCyd treatment and monitor therapy effectiveness.

DISCLOSURE

ACKNOWLEDGMENTS

REFERENCES

1. Lapeyre JN, Becker FF. 5-methylcytosine content of nuclear DNA during chemical hepatocarcinogenesis and in carcinomas which result. *Biochem Biophys Res Commun.* 1979;87:698–705.
2. Heerboth S, Lapinska K, Snyder N, et al. Use of epigenetic drugs in disease: an overview. *Genet Epigenet.* 2014;6:9–19.
3. Kelly TK, De Carvalho DD, Jones PA. Epigenetic modifications as therapeutic targets. *Nat Biotechnol.* 2010;28:1069–1078.
4. Smith SS, Kaplan BE, Sowers LC, Newman EM. Mechanism of human methyl-directed DNA methyltransferase and the fidelity of cytosine methylation. *Proc Natl Acad Sci USA.* 1992;89:4744–4748.
5. Newman EM, Santi DV. Metabolism and mechanism of action of 5-fluorodeoxycytidine. *Proc Natl Acad Sci USA.* 1982;79:6419–6423.
6. Ho DH. Distribution of kinase and deaminase of 1-beta-D-arabinofuranosylcytosine in tissues of man and mouse. *Cancer Res.* 1973;33:2816–2820.
7. Maehara Y, Nakamura H, Nakane Y, et al. Activities of various enzymes of pyrimidine nucleotide and DNA syntheses in normal and neoplastic human tissues. *Gan.* 1982;73:289–298.
8. Ahmed M, Cannon DM, Scanlon C, et al. Progressive brain atrophy and cortical thinning in schizophrenia after commencing clozapine treatment. *Neuropsychopharmacology.* 2015;40:2409–2417.
9. Beumer JH, Eiseman JL, Parise RA, et al. Plasma pharmacokinetics and oral bioavailability of 3,4,5,6-tetrahydrouridine, a cytidine deaminase inhibitor, in mice. *Cancer Chemother Pharmacol.* 2008;62:457–464.
10. Holleran JL, Beumer JH, McCormick DL, et al. Oral and intravenous pharmacokinetics of 5-fluoro-2′-deoxycytidine and THU in cynomolgus monkeys and humans. *Cancer Chemother Pharmacol.* 2015;76:803–811.
11. Morfouace M, Nimmervoll B, Boulos N, et al. Preclinical studies of 5-fluoro-2′-deoxycytidine and tetrahydrouridine in pediatric brain tumors. *J Neurooncol.* 2016; 126:225–234.
12. Yoshida M, Hoshi A, Kuretani K, Saneyoshi M. Mode of action of 5-fluorocytidine and 5-fluoro-2′-deoxycytidine in L5178Y cells in vitro. *Chem Pharm Bull (Tokyo).* 1982;30:1018–1023.
13. Newman EM, Morgan RJ, Kummar S, et al. A phase I, pharmacokinetic, and pharmacodynamic evaluation of the DNA methyltransferase inhibitor 5-fluoro-2′-deoxycytidine, administered with tetrahydrouridine. *Cancer Chemother Pharmacol.* 2015;75:537–546.
14. Valdespino V, Valdespino PM. Potential of epigenetic therapies in the management of solid tumors. *Cancer Manag Res.* 2015;7:241–251.
15. Kelly AD, Kroeger H, Yamazaki J, et al. A CpG island methylator phenotype in acute myeloid leukemia independent of IDH mutations and associated with a favorable outcome. *Leukemia.* 2017;31:2011–2019.
16. Beumer JH, Parise RA, Newman EM, et al. Concentrations of the DNA methyltransferase inhibitor 5-fluoro-2′-deoxycytidine (FdCyd) and its cytotoxic metabolites in plasma of patients treated with FdCyd and tetrahydrouridine (THU). *Cancer Chemother Pharmacol.* 2008;62:363–368.
17. Ryu YH, Liow JS, Zoghbi S, et al. Disulfiram inhibits defluorination of ^{18}F-FCWAY, reduces bone radioactivity, and enhances visualization of radioligand binding to serotonin 5-HT1A receptors in human brain. *J Nucl Med.* 2007;48: 1154–1161.
18. Hays MT, Watson EE, Thomas SR, Stabin M. MIRD dose estimate report no. 19: radiation absorbed dose estimates from ^{18}F-FDG. *J Nucl Med.* 2002;43:210–214.
19. Delbeke D, Coleman RE, Guiberteau MJ, et al. Procedure guideline for tumor imaging with ^{18}F-FDG PET/CT 1.0. *J Nucl Med.* 2006;47:885–895.
20. Zanzonico PB, Finn R, Pentlow KS, et al. PET-based radiation dosimetry in man of ^{18}F-fluorodihydrotestosterone, a new radiotracer for imaging prostate cancer. *J Nucl Med.* 2004;45:1966–1971.
21. Erdi YE. Limits of tumor detectability in nuclear medicine and PET. *Mol Imaging Radionucl Ther.* 2012;21:23–28.
22. Adler S, Seidel J, Choyke P, et al. Minimum lesion detectability as a measure of PET system performance. *EJNMMI Phys.* 2017;4:13.